

New Modeling of the Lensing Galaxy and Cluster of Q0957+561: Implications for the Global Value of the Hubble Constant

Kyu-Hyun Chae

Department of Physics & Astronomy, University of Pittsburgh, Pittsburgh, PA 15260

ABSTRACT

The gravitational lens 0957+561 is modeled utilizing recent observations of the galaxy and the cluster as well as previous VLBI radio data which have been re-analyzed recently. The galaxy is modeled by a power-law elliptical mass density with a small core while the cluster is modeled by a non-singular power-law sphere as indicated by recent observations. Using all of the current available data, the best-fit model has $\chi^2_{\min}/N_{\text{dof}} \approx 6$ where the χ^2 value is dominated by a small portion of the observational constraints used; this value of the reduced χ^2 is similar to that of the recent FGSE best-fit model by Barkana et al. However, the derived value of the Hubble constant is significantly different from the value derived from the FGSE model. We find that the value of the Hubble constant is given by $H_0 = 69^{+18}_{-12}(1 - \kappa)$ and $74^{+18}_{-17}(1 - \kappa)$ km s $^{-1}$ Mpc $^{-1}$ with and without a constraint on the cluster's mass, respectively, where κ is the convergence of the cluster at the position of the galaxy and the range for each value is defined by $\Delta\chi^2 = \chi^2_{\min}/N_{\text{dof}}$. Presently, the best achievable fit for this system is not as good as for PG 1115+080, which also has recently been used to constrain the Hubble constant, and the degeneracy is large. Possibilities for improving the fit and reducing the degeneracy are discussed.

Subject headings: gravitational lensing — distance scale — quasars: individual (Q0957+561)

1. Introduction

The gravitationally lensed “double quasar” Q0957+561 is the first lensed system for which time delay between image components has been measured with considerable confidence and accuracy (Haarsma et al. 1999; Pelt et al. 1998; Kundić et al. 1997; Pijpers 1997; Oscoz et al. 1997; Schild & Thomson 1997). In principle, the measured time delay (417 ± 3 d, Kundić et al. 1997) can be turned into an accurate determination of the Hubble constant, H_0 , using the method outlined by Refsdal (1964, 1966; see Schneider, Ehlers, & Falco 1992 for a pedagogical introduction). For this, the potential of the lens (i.e. its mass distribution) must be well-determined consistent with

observational constraints. Many important observational constraints on Q0957+561 have come from the VLBI observations of the radio jets and cores of the two image components (Garrett et al. 1994; Gorenstein et al. 1988; Gorenstein et al. 1984). The Garrett et al. (1994) data have been re-analyzed just recently and improved constraints are given by Barkana et al. (1999, hereafter Ba99).

The lensing of Q0957+561 is due to the combined effect of a massive elliptical galaxy and a cluster at redshift $z = 0.36$ of which the elliptical galaxy is the brightest member. The cluster has been studied using optical observations (Angonin-Willaime, Soucail, & Vanderriest 1994; Garrett, Walsh, & Carswell 1992), X-ray observations (Chartas et al. 1998; Chartas et al. 1995), and weak lensing effects (Fischer et al. 1997; Dahle, Maddox, & Lilje 1994). These studies indicate that the lensing galaxy is positioned close to the center of the cluster, and the cluster's convergence in the region of the image is significant. However, the cluster's mass distribution could not be accurately determined from those studies. The lensing galaxy has been detected both optically (Bernstein et al. 1997, hereafter Be97; Stockton 1980) and in the radio (Roberts et al. 1985; Gorenstein et al. 1983). The more recent HST observations by Be97 appear to have significantly reduced the uncertainty in the position of the galaxy. The HST optical position (G1) is consistent with the VLBI position (G'), but is inconsistent with the VLA position (G). The Be97 observations also reveal new possible lensed features of two blobs and two knots along with an arc in the system.

Present observational constraints (the VLBI and HST constraints) now clearly exclude both the Grogin & Narayan (1996) softened power-law sphere (SPLS) model and the Falco, Gorenstein, & Shapiro (1991) model (FGS) of a King profile sphere with a central black hole, which were previously the best-fit models. Ba99 extended the SPLS and FGS models to include an arbitrary ellipticity to the galaxy, and the new versions of models [softened power-law elliptical mass distribution (SPEMD) and FGSE] fit the observations better. According to their study, the FGSE model gives a somewhat better fit than the SPEMD model [$\bar{\chi}^2_{\min} (\equiv \chi^2_{\min}/N_{\text{dof}}) \approx 6$ vs. 10]. Notably, the value of H_0 derived from the FGSE model is $\gtrsim 100 \text{ km s}^{-1} \text{ Mpc}^{-1}$. In previous models of Q0957+561, the lensing cluster has been modeled by a quadrupole term (e.g. Ba99; Grogin & Narayan 1996; Falco, Gorenstein, & Shapiro 1991) because of its simplicity and assuming that higher order terms can be neglected in the expansion of the cluster potential. In addition, Ba99 considered a singular isothermal sphere (SIS) to model the cluster for the FGSE model of the galaxy while Bernstein & Fischer (1999) considered higher order terms in the cluster expansion. Ba99 found that for the FGSE model of the galaxy, a SIS model of the cluster did not lead either to an improved $\bar{\chi}^2_{\min}$ or a significantly different value of H_0 compared with the case using a quadrupole term. Thus, for the FGSE model of the galaxy, it appears that consideration of a realistic cluster mass model is not crucial. However, the quadrupole term alone may not accurately account for the cluster contribution, especially since recent observations indicate the cluster's mass center can be very close to the galaxy (Fischer et al. 1997; Angonin-Willaime et al. 1994), and there is no *a priori* reason that we need only consider the SIS model for the cluster. Bernstein & Fischer's (1999) consideration of higher-order terms can be a better approximation of

the cluster potential than the single quadrupole term, however, the low χ^2 values of their best-fit models depended, in large part, on their selective use of the current observational constraints (see §5).

In this study we consider a more general model of the cluster, i.e., a power-law sphere while modeling the galaxy with a power-law elliptical mass density with a small core [i.e. the SPEMD model with a fixed small core (see §2 and §3)]. We also consider the case where the cluster is elliptical. The reduced χ^2 of the best-fit model of this type is similar to that of the best-fit FGSE model. However, the derived value of H_0 is significantly different from the value derived from the FGSE model. It turns out that neither the core radius nor the power-law radial index of the cluster can be determined from fitting the model to the current observational constraints. This is because the variation of either the radial index or the core radius (within a wide range) does not significantly alter the fit, while the convergence of the cluster (κ) at the position of the galaxy (and thus the derived value of H_0) varies. Thus, we can only derive a scaled [by a factor of $(1 - \kappa)$] value of H_0 . The outline of this paper is as follows. We first review the adopted observational constraints (§2). In §3, we present the lens model and review its parameters. In §4, we present the results of fitting the model to the observational constraints, and derive a value for H_0 . In §5, we discuss possible future improvements to the determination of H_0 using the Q0957+561 lens.

2. Summary of Current Observational Constraints

The optical image of Q0957+561 consists of two point-like quasars A and B $\approx 6''$ apart on the sky. This is only a weak constraint on a lens model. However, the radio image of Q0957+561 provides many strong constraints. In particular, the extended radio jets along with the radio cores can be used to derive both accurate relative positions of the jets with respect to their cores and between the cores, and relative magnification matrix between the corresponding components of A and B. The separation between the cores was measured with an uncertainty of $0''.00004$ using VLBI observations (Gorenstein et al. 1984; Falco et al. 1991). Further VLBI observations at $\lambda = 13$ cm by Gorenstein et al. (1988) identified three jets in each quasar, which were used to derive a relative magnification matrix $[\mathbf{M}_{BA}] = [\partial \mathbf{x}_B / \partial \mathbf{x}_A]$ between quasars A and B. More recently, VLBI observations at $\lambda = 18$ cm by Garrett et al. (1994) separated the jets into five components for each quasar, from which they derived an improved relative magnification matrix along with its gradient. However, Ba99 employed improved analysis procedures to re-analyze the raw data of Garrett et al. (1994), in particular, they corrected some significant errors in the VLBI data reduction packages adopted by Garrett et al. (1994) and fitted the jet component parameters (i.e. positions, fluxes, and Gaussian model parameters) and the magnification transformation parameters simultaneously in a single step, and so we will use the constraints given by Ba99 in this study.

Radio observations of the system have resulted in the detection of radio sources near the

optical center of the lensing galaxy (Roberts et al. 1985; Gorenstein et al. 1983). While both the VLA position G (Roberts et al. 1985) and the VLBI position G' (Gorenstein et al. 1983) were reported to have an uncertainty of 1 mas, they differed 30σ from each other. The optical position (G1) of the lensing galaxy as measured by Stockton (1980) is more consistent with the VLBI position, however, his measurement uncertainty is large (30 mas). Thus, in previous studies which modeled the lens, it was not clear which observed position to use as a constraint. However, HST observations of the system by Be97 were used to determine the optical position of the lensing galaxy with an uncertainty of 3.5 mas. The HST position is consistent with the VLBI position within 10 mas, but it is clearly inconsistent with the VLA position. Whether the HST position or the VLBI position are used to constrain the lens model (§4) makes little difference; however we will use the VLBI position. Another constraint to be used is the core flux ratio B/A derived from VLBI/VLA observations and observations of the optical emission lines (Conner, Lehár, & Burke 1992; Schild & Smith 1991). The above constraints, derived mostly from VLBI observations, are used as our “primary constraints” [we mean by this that these constraints have been derived from confirmed lensed features, and that they are used in the first step of the fitting procedure (see §3)] on the lens model; they are summarized in Table 1.

The Be97 HST observations detected possible lensed images of other background sources. Blobs 2 & 3 are probably images of a common background galaxy. Knots 1 & 2, which form an arc, are also probably images of a common source. While a lens model which is based on the primary constraints easily satisfies the constraints from the knots, the constraints from the blobs turn out to be useful for distinguishing between models. The constraints from the blobs and knots are used as “secondary constraints” which are summarized in Table 4. The total number of primary and secondary constraints is 25. All of these constraints are used to define the “goodness of fit”, χ^2 , taking into account correlation coefficients for some constraints (Table 2 and Table 3).

Another observational constraint is the upper limit on the relative brightness of any third image (image “C”) which is predicted by a lens model that has a smooth mass distribution at the central region of the galaxy. The VLBI observations by Gorenstein et al. (1984) put a 5σ upper limit of $C/B = 3.3\%$ while the optical observations by Stockton (1980) found $C/B < 2\%$. The relative brightness of the third image is mostly related to the mass distribution at the central region of the lens, which is effectively described by a core radius parameter. The observed low values of the upper limit on the relative brightness of a third image implies that the core radius of the lens model is very small (see §3). If the core radius is sufficiently small, then the lensing properties of the model become insensitive to the value of the core radius, since mass distributions with different core radii (and different central densities) are essentially the same outside the small central regions. Thus, we can fix the core radius at a small value which ensures that the relative magnification of the third image predicted by the model is always less than the observational upper limit. This approach is employed in this study.

3. An Observationally Motivated Model of the Lens

We consider the following forms for the mass distributions of the lensing galaxy

$$\Sigma_{\text{gal}}(r, \theta) = \frac{\Sigma_1}{\left\{1 + \left(\frac{r}{r_1}\right)^2 [1 + e_1 \cos 2(\theta - \theta_1)]\right\}^{(\nu_1-1)/2}} \quad (1)$$

and cluster

$$\Sigma_{\text{cl}}(r') = \frac{\Sigma_2}{\left\{1 + \left(\frac{r'}{r_2}\right)^2\right\}^{(\nu_2-1)/2}}. \quad (2)$$

Here Σ_i ($i = 1, 2$) are the central surface mass densities, r_i are the core radii, and ν_i are the radial indices. Radial index $\nu = 1, 2$, and 3 correspond to radial profiles of constant surface density, isothermal, and modified Hubble law, respectively, so that it is related to the parameter η used by Grogin & Narayan (1996) and Ba99 via $\nu = 3 - \eta$. The parameter e_1 (> 0) is related to the galaxy's ellipticity ϵ_1 ($\equiv 1 - b/a$ where a, b are the major, minor axes respectively) via $\epsilon_1 = 1 - [(1 - e_1)/(1 + e_1)]^{1/2}$. The parameter θ_1 is the position angle (north through east) of the galaxy. Primed coordinates are used for the cluster's mass distribution since the cluster's center is off from the galaxy's center. The relative position of the cluster with respect to the galaxy is represented by the distance between them, d_{12} , and the position angle of the cluster's center as viewed from the galaxy, PA_{12} . The above model will be referred to as “PEM+PS” (meaning Power-law Elliptical Mass + Power-law Sphere) model.

Throughout we assume a standard cosmology with a cosmological matter-energy parameter $\Omega_{\text{Matter}} = 1$ and a cosmological vacuum-energy parameter $\Omega_{\Lambda} = 0$, and we use the usual definition $h = H_0/100 \text{ km s}^{-1} \text{ Mpc}^{-1}$. For this choice of cosmology we have $1'' \approx 3.0h^{-1} \text{ kpc}$ at the redshift of the lens. For an open universe with $\Omega_{\text{Matter}} = 0.3$ (and $\Omega_{\Lambda} = 0$), an estimate of h increases by $\approx 7\%$. As explained in §2, the present observational constraint on the relative brightness of a third image implies that the core radius of the galaxy, r_1 , should be very small. For example, the upper limit on the core radius of a galaxy with radial index $\nu_1 = 1.72$ in equation (1) is $r_1 \approx 10h^{-1} \text{ pc}$ for $\text{C/B} \leq 3.3\%$. We fix the core radius at $r_1 = 0.1h^{-1} \text{ pc}$, which is small enough to satisfy the observational constraint for any value of ν_1 , but is an arbitrary choice otherwise (see §2). The other parameters of the galaxy (i.e. central density, ellipticity, and position angle) are free parameters for the model. Thus, our model of the lensing galaxy can be considered as a dark matter dominated mass model. It will be interesting to compare the determined mass distribution of the lensing galaxy with its observed light distribution (Be97).

Present observational studies of the lensing cluster indicate that the cluster's mass distribution is more consistent with an extended core (Chartas et al. 1998; Fischer et al. 1997), although the uncertainties in the derived values are too large for them to be directly used to constrain the lens model. Thus, we fix the core radius at an arbitrary large value (e.g. several arcseconds) and derive a value of h with the fixed core radius. And then, we study how the derived value of h is affected

if we vary the core radius from the chosen value. There is no observational constraint on the radial index of the cluster. Thus, we fix the radial index at an arbitrary value, e.g., $\nu_2 = 2$ (isothermal profile), and then study how the derived value of h is affected when ν_2 is varied.

To calculate the lensing properties (i.e. deflection, magnification, and relative light travel time) of the mass distribution implied by equation (1) we use the series method by Chae, Khersonsky, & Turnshek (1998); for the details, the reader is referred to the paper and references therein. In fitting the observational constraints of Q0957+561, we must use an accurate and robust method of calculation since the fractional errors of the VLBI data are as small as $\sim 10^{-5}$. The calculational accuracy of the series method can be made orders of magnitude smaller than the observational errors by controlling the truncation of the series. This was tested for the isothermal case of $\nu = 2$ using the analytic solution of Kormann, Schneider, & Bartelmann (1994).¹ Since the series converge well for an arbitrary value of ν , we can be confident that the series calculation gives sufficiently accurate results. Given that the total number of constraints is 25 and the total number of free parameters [including the eight coordinates of the four sources (i.e. core, jet, blob and knot) and two redshifts of the blob and knot] is 17, the minimization of the χ^2 is not a simple numerical task. For this reason, we first fit the model to the primary constraints only, so that we can work with smaller numbers of constraints and free parameters. Once best-fit values based on the primary constraints are determined, the secondary constraints and the remaining parameters are considered, and then the entire set of parameters are adjusted to minimize the χ^2 .

4. Results of Fitting the Model to the Observational Constraints: Bounds on the Hubble Constant

Because of the degeneracies in the cluster's core radius (r_2) and radial index (ν_2), we first consider fixed values of r_2 and ν_2 , and then study how varying them affects the derivation of h . We set $\nu_2 = 2$ and $r_2 = 15h^{-1}$ kpc ($\approx 5''$). We find that the model has significant degeneracies in parameters ν_1 (the galaxy's radial index) and d_{12} (the separation between the cluster and the galaxy). Thus, we fix the parameters ν_1 and d_{12} for each model and, by incrementing them in steps of 0.02 and 1" respectively, obtain a grid of models in the 2-dimensional parameter space spanned by ν_1 and d_{12} . A model with $\nu_1 = 1.72$ and $d_{12} = 9''$ has the lowest value of χ^2 of $\chi^2_{\min} \approx 49.6$ with 8 degrees of freedom ($\bar{\chi}^2_{\min} \approx 6.2$). As the parameters ν_1 and d_{12} are varied from the best-fit values, χ^2 increases moderately. A confidence limit (CL) ellipse defined by $\Delta\chi^2 = \bar{\chi}^2_{\min}$ is shown in Figure 1 (full line). Although this results in a larger region of parameter space than the conventional 1σ (i.e. 68% CL) region, we adopt it as in Ba99 and Grogin & Narayan (1996) since the best-fit model has a poor overall χ^2 .

¹The calculational accuracy of the series method depends on the value of the core radius. For our chosen value of $r_c = 10^{-4}h^{-1}$ kpc, the fractional calculational errors are $\sim 10^{-9}$ to 10^{-7} for $\epsilon \lesssim 0.5$.

For the best-fit model ($\nu_1 = 1.72$, $d_{12} = 9''$), we find $h = 0.54$ which is obtained from $h = \Delta\tau_{\text{AB}}^{(\text{model})}/\Delta\tau_{\text{AB}}^{(\text{observed})} = (225 \text{ d})/(417 \text{ d}) = 0.54$, where $\Delta\tau_{\text{AB}}^{(\text{model})}$ is calculated for $H_0 = 100 \text{ km s}^{-1} \text{ Mpc}^{-1}$. In the $\Delta\chi^2 = \bar{\chi}_{\text{min}}^2$ range, $0.39 < h < 0.70$. However, this value of h was obtained for the fixed cluster parameters of $\nu_2 = 2$ and $r_2 = 15h^{-1} \text{ kpc}$. Although these choices are the best values obtained by Fischer et al. (1997), their allowed range of r_2 is large, and there is no *a priori* reason that the cluster’s mass distribution should have an exact isothermal profile. Thus, we must study how the above derived value of h is affected as the cluster parameters are varied. The effect of varying the cluster’s radial index turns out to be trivial; for a profile shallower ($\nu_2 < 2$) or steeper ($\nu_2 > 2$) than the isothermal, the fit results are virtually the same except that the cluster’s convergence at the position of the galaxy (κ), i.e. at $r = 0$, is altered and the value of h is scaled by a factor of the ratio of the values of $(1 - \kappa)$. In Figure 2 are shown the values of $(\chi^2, h/(1 - \kappa), \kappa)$ for various example cluster parameter sets. We see that for a wide range of $1.5 \leq \nu_2 \leq 2.5$ around the isothermal value ($\nu_2 = 2$) at core radius $r_2 = 15h^{-1} \text{ kpc} (\approx 5'')$, $\Delta\chi^2 < 0.12\bar{\chi}_{\text{min}}^2$ and $h/(1 - \kappa)$ changes by no larger than 1.4% while $\Delta\kappa > 0.22$. The effect of varying the cluster’s core radius can be more complicated. Nevertheless, we find that for the observational range of r_2 by Fischer et al. (1997), the effect is simple (see Fig. 2). Namely, when the core radius is increased or decreased from $r_2 \approx 5''$ for the isothermal profile, the χ^2 varies little ($\Delta\chi^2 < 0.18\bar{\chi}_{\text{min}}^2$), the value of κ is altered, and the value of h scales, to a good approximation (up to an error of 2.8%), according to $(1 - \kappa)$ for $0 \lesssim r_2 \lesssim 10''$. In summary, for a range of the cluster’s radial index and core radius ($1.5 \leq \nu_2 \leq 2.5$, $0 \lesssim r_2 \lesssim 10''$) which we investigated with the current observational constraints, we find that there is no significant change of χ^2 ($\Delta\chi^2 < 0.26\bar{\chi}_{\text{min}}^2$), and that the change of h is dictated by $(1 - \kappa)$ to an error no larger than $\approx 4\%$. Therefore, the mass-sheet degeneracy (Falco, Gorenstein, & Shapiro 1985) appears to persist even when we use a full potential model of the cluster. (We remind ourselves that when the quadrupole approximation was adopted in previous lens models of Q0957+561, this degeneracy was exact.)

However, for each radial profile of the cluster, the χ^2 has a “minimum” value at a certain finite core radius (e.g. at $r_2 \approx 2''$ for the isothermal case) and the χ^2 increases consistently as the core radius is varied, although we concluded above that the variation of the χ^2 was insignificant with the current observational constraints. There is a subtlety here. Even though the total χ^2 remains virtually invariant as the core radius is varied for a fixed radial index, the χ^2 contributions due to the primary constraints and those due to the secondary constraints vary significantly. For instance, for the isothermal profile ($\nu_2 = 2$), the model with $r_2 \approx 0''$ has $\chi_p^2 \approx 35.6$ and $\chi_s^2 \approx 14.0$ while the model with $r_2 \approx 10''$ has $\chi_p^2 \approx 40.2$ and $\chi_s^2 \approx 10.2$, where χ_p^2 and χ_s^2 denote the χ^2 contributions due to the primary and secondary constraints, respectively. As will be seen in §5, the radio jet positions have the largest χ^2 contribution out of the the primary constraints, so does the blob magnification ratio out of the secondary constraints. This suggests that better observational knowledge of the radio jets and the blob magnification ratio could break the present “superficial” degeneracy of the core radius for a given value of the radial index. When the radial index is varied for a fixed value of the core radius, the χ_p^2 and χ_s^2 each change by only ≈ 1 for $\Delta\nu = 1$. This means that the degeneracy of the cluster’s radial index is much more significant

with the present observational constraints. Unless new independent observational constraints are revealed, the degeneracy of the cluster’s radial index could not be broken.

As seen in the above, the degeneracy of the cluster’s core radius is weaker than that of the cluster’s radial index. However, the determination of $h/(1 - \kappa)$ is not significantly affected by varying the core radius. To illustrate this, CL ellipses are drawn in Fig. 1 for two other values of r_2 , i.e., $r_2 \approx 3''$ (dashed line) and $r_2 \approx 7''$ (dotted line). As seen in the figure, confidence region of the parameter space is altered only slightly whether as the core radius is increased or decreased. The $\Delta\chi^2 = \bar{\chi}_{\min}^2$ range of $h/(1 - \kappa)$ is nearly unchanged for $0 \lesssim r_2 \lesssim 10''$. From the grid of models with $\nu_2 = 2$ and $r_2 = 15h^{-1}$ kpc ($\approx 5''$), we find $h = 0.74_{-0.17}^{+0.18}(1 - \kappa)$.

As we considered a CL by $\Delta\chi^2 = \bar{\chi}_{\min}^2$ in the above, we could consider a CL by $\Delta\chi^2 = 4\bar{\chi}_{\min}^2$. However, the confidence region within so defined a CL is too large to be useful to constrain h . If the cluster’s mass is constrained, the ranges of the parameter space can be reduced. Unfortunately, the cluster’s mass is not well-determined from present observations. Figure 3 shows confidence regions of the parameter space of the model with $\nu_2 = 2$ and $r_2 = 15h^{-1}$ kpc including the cluster’s mass as a constraint determined directly from weak lensing effects by Fischer et al. (1997; $\Sigma_0 = 0.36 \pm 0.11h \times 10^{10} M_\odot \text{ kpc}^{-2}$ for $\nu = 2$ and $r_c \approx 5''$).² The parameter space is slightly better constrained compared with the case that the cluster’s mass is not constrained (Fig. 1). We find $\bar{\chi}_{\min}^2 \approx 5.6$ for $\nu_1 = 1.70$ and $d_{12} = 10''$. The derived value of the Hubble constant is $h = 0.69_{-0.12}^{+0.18}(1 - \kappa)$ with the cluster’s mass constrained. The measured velocity dispersions of the lensing galaxy (Tonry & Franx 1998; Falco et al. 1997; Rhee 1991) can, in principle, be used to constrain the mass of the galaxy, which can be useful for reducing the degeneracy in the parameter space of the PEM+PS model. Stellar orbit modeling methods have been applied to the best-fit SPLS mass profile of Grogan & Narayan (1996) to infer the mass of the galaxy (Romanowsky & Kochanek 1999). Similar studies in the future for the PEM galaxy model could be useful.

Table 5 summarizes the values of the parameters for the model with $\nu_2 = 2$ and $r_2 = 15h^{-1}$ kpc with the cluster’s mass unconstrained. The theoretical images of the radio core and the brightest radio jet for the best-fit model are shown in Figure 4. Figure 5 shows theoretical images of the optical blob and knot along with an arc. The model galaxy’s radial profile is somewhat shallower than the isothermal profile $\nu = 2$, i.e., the mass within radius r increases faster than the isothermal case as r increases. The model galaxy’s ellipticity ($\epsilon_{\text{model}} \approx 0.01$ to 0.38) is similar to the ellipticity of the observed light ($\epsilon_{\text{light}} \approx 0.05$ to 0.49 ; Be97). The observed position angle of the light distribution is $\text{PA}_{\text{light}} \approx 32^\circ$ to 68° (Be97). The position angle of the best-fit model ($\text{PA}_{\text{model}} = 64^\circ$) is in agreement with the light distribution. However, in the $\Delta\chi^2 = \bar{\chi}_{\min}^2$ range, $6^\circ \lesssim \text{PA}_{\text{model}} \lesssim 166^\circ$. Here it is interesting to note that for the majority of 17 gravitational lens galaxies studied by Keeton, Kochanek, & Falco (1998), the position angles of the light and the mass (i.e. lens model) are the same to $\lesssim 10^\circ$. In other words, not all of the models within the

²Here we do not constrain the cluster’s positions, and thus we do not constrain the cluster’s convergence at $r = 0$ although we do constrain its mass.

$\Delta\chi^2 = \bar{\chi}_{\min}^2$ range around the best-fit model are consistent with the general result obtained by Keeton et al. (1998), and this in turn implies that the derived range of the Hubble constant would be narrower than obtained above if we required the model position angle to be in agreement with the light position angle. [If a quadrupole term were used to account for the cluster contribution, PA_{model} would be $\sim -40^\circ$ (or, 140°) implying that the dark matter be oriented nearly orthogonal to the light in contrast to our best-fit model and the general result of Keeton et al. (1998).] The predicted position of the cluster’s mass center off from the galaxy is in the northeast direction consistent with the Fischer et al. (1997) determination and the prediction of the FGSE+SIS model by Ba99. The PEM+PS model predicts that the cluster’s center of mass is closer to the galaxy than, and the cluster is less massive than Fischer et al. (1997) found.

Since the lowest $\bar{\chi}^2$ of the PEM+PS model is not very good, we are led to consider a possibility of elliptical mass distribution for the cluster. We find that χ_{\min}^2 decreases slightly if an ellipticity is given to the cluster, but $\bar{\chi}_{\min}^2$ worsens. Moreover, this has little effect on the derived value of H_0 . The result of the fit shows that the cluster would be oriented to the north if it is elliptical (i.e. $\text{PA}_{\text{cluster}} \sim 0^\circ$). Finally, we consider allowing the lensing galaxy’s positions to be free parameters. In this case, the observed light distribution is completely ignored. In particular, it is assumed that the center of mass could be very different from the position of the centroid of the light. We find that the lowest $\bar{\chi}^2$ improves to $\bar{\chi}_{\min}^2 \approx 4.7$ ($\chi_{\min}^2 \approx 28$), but the derived value of H_0 is unaffected if the lensing galaxy’s positions are free parameters. The modeled lens positions relative to the VLBI positions of G' are $\Delta\text{RA} = 28$ mas and $\Delta\text{Dec} = -97$ mas.

5. Discussion

Recent observations of the lensing galaxy and cluster of Q0957+561 (Be97; Fischer et al. 1997) motivated modeling the galaxy by an elliptical mass distribution and modeling the cluster by a power-law sphere with an extended core. The PEM+PS model (§3) was fitted to both the VLBI constraints (Ba99) and the HST constraints (Be97) of the system to derive a value for H_0 . The best-fit model has $\bar{\chi}_{\min}^2 \approx 6$ which is better than the best-fits achievable by previous models. Here it should be emphasized that the relative improvement of the fit was achieved by using an elliptical mass distribution for the galaxy *and* using a mass sphere for the cluster, replacing the quadrupole term. The only other model which gives a fit of comparable quality is the FGSE model of Ba99, where the galaxy is modeled by an elliptical King profile mass distribution with an extended core along with a large effective black hole (BH) mass at the galaxy’s center, while the cluster is modeled using a quadrupole term or a singular isothermal sphere (SIS). The FGSE model suggests that the Hubble constant is $h = 1.23_{-0.23}^{+0.22}$ and $1.13_{-0.27}^{+0.32}$ ($\Delta\chi^2 = 4\bar{\chi}_{\min}^2$ CLs) using the quadrupole term and the SIS for the cluster, respectively. A few comments appear to be relevant regarding the FGSE model. First, the model requires a very large point mass of $\sim 10^{11} \text{ M}_\odot$, which does not seem observationally motivated or supported. Second, the value of H_0 derived from

the FGSE model is inconsistent with other recent independent determinations of H_0 , especially the determination by Impey et al. (1998) from the lens PG 1115+080, who found $h \lesssim 0.70$ regardless of the choice of lens models. On the other hand, the PEM+PS model predicts that $h = 0.69_{-0.12}^{+0.18}(1 - \kappa)$ and $0.74_{-0.17}^{+0.18}(1 - \kappa)$ ($\Delta\chi^2 = \bar{\chi}_{\min}^2$ CLs) with the cluster's mass constrained and unconstrained, respectively. Since $\kappa > 0$, the PEM+PS model predicts a significantly lower value for the Hubble constant than the FGSE model. Just recently, Bernstein & Fischer (1999) have considered breaking power-law index of the galaxy to model its potential by up to 3 subregions of independent elliptical mass distribution, and have included higher-order-than-quadrupole terms in the multipole expansion of the cluster potential. Although Bernstein & Fischer's (1999) models are more sophisticated than previous (published) models and their models give $\chi^2 \sim N_{\text{dof}}$, direct comparison with the above models (i.e. PEM+PS, FGSE) is not possible because they did not use the full set of magnification constraints (but used only the flux ratios) and de-emphasized the observed jet positions by using $\approx 5\sigma$ in the definition of their χ^2 , and because of other differences in the fit procedure, e.g., their fixing the redshifts of the blobs and knots at $z = 1.41$, calculating the positional χ^2 on the source plane by transforming the image position variances to it.³ They have found $h = 1.04_{-0.23}^{+0.31}(1 - \kappa)$ (95% CL).

The mere values of $\bar{\chi}_{\min}^2$ of the FGSE model and the PEM+PS model cannot distinguish between them. Even worse, neither of the models can be considered to be acceptable if the adopted observational errors are true and assumed normally distributed, even though they give present “best” fits. In other words, we are at present faced with two difficulties in determining H_0 from the Q0957+561 lens. One is the poor fit of the present best models to the present observational constraints. This might be, from a modeler's point of view, partly because the reported measurement errors were underestimated and/or possible systematic errors (see below) could not be taken into account. In fact, Ba99 point out that the radio jet positions and the magnification constraints, derived from the VLBI data using even the improved analysis procedure, should be treated with some caution. For example, superluminal motion over the period of the time delay or a milli-arcsecond scale deflection by a globular cluster could have influenced the observed jet positions by a scale much larger than their formal uncertainties of ~ 0.1 mas. For this reason, it is useful to identify the individual contributions of the observational constraints to the total χ^2 . Table 6 shows the χ^2 contributions of the observational constraints for the PEM+PS model. Remarkably, the jet positions contribute most to the χ^2 , and they have the second largest $\chi^2/N_{\text{constraint}}$ after the blob magnification ratio.⁴ This could be an indication that

³Using the same constraints used by Bernstein & Fischer (1999), but calculating the positional χ^2 on the image plane (thus with no approximations) and allowing the redshifts of the blobs and knots each to be free parameters, we find, for example, that a PEM+PS model with $\nu_1 = 1.86$ and $d_{12} = 4''$ have $\chi^2 \approx 10$ with $N_{\text{dof}} = 4$ which is comparable, in the fit quality, to the the best-fit models of Bernstein & Fischer (1999).

⁴The large χ^2 contribution of the blob magnification ratio might not be a surprising result since current data on the blobs' surface brightnesses do not permit a very reliable estimate of the centroid magnification ratio (Bernstein 1998, private communication).

the above-mentioned effects are present. Nonetheless, the poor overall fit is an indication that more sophisticated and realistic models need to be considered in the future to better describe the mass distribution of the lens. As seen in §4, the introduction of an ellipticity to the cluster does not improve $\bar{\chi}^2_{\min}$, at least with the present observational constraints.

Up until now in lens research, an elliptical mass density of a constant ellipticity [e.g. the functional form of eq. (1)] has been used, as regarded relatively realistic, to model a lensing object. While the mass distribution of equation (1) is very flexible in that all of its parameters are unrestricted, it has several limitations in describing the true mass distribution of a lensing object, e.g., the elliptical lensing galaxy of Q0957+561. First, a truncation radius is not included in its functional form. For this reason its total mass diverges for a radial profile not steeper than the modified Hubble profile (i.e. for $\nu \leq 3$). Second, the ellipticity of equation (1) is constant over the entire range of r . The observed light distribution of the lensing galaxy in Q0957+561 (Be97) shows a varying ellipticity as a function of r in the inner region of the galaxy. Even when dark mass is the dominant mass component, it would be surprising if the ellipticity of the mass distribution was constant over the entire range of r . Third, the position angle of equation (1) is constant over the entire range of r . We note that the observed position angle of the lensing galaxy in Q0957+561 (Be97) is scattered for a range of r . Finally, equation (1) neglects small scale perturbations or substructure (Mao & Schneider 1998) but assumes a smooth distribution of mass. Bernstein & Fischer's (1999) models partly account for the second and third points, however, the evaluation of their models depends on interpretation of the current observational constraints. Realistic incorporation of the above-mentioned deviations from equation (1) may improve the fit unambiguously in the future.

In this and previous studies (Ba99; Grogin & Narayan 1996), attempts have been made to put constraints on H_0 using lens models despite the poor fits. We are faced with another difficulty in those attempts; two classes of models with similar quality fits can give disagreeing values of H_0 , and the range of H_0 for each class of model is large. This “degeneracy problem” was also encountered in the recent efforts to determine H_0 using the lens PG 1115+080 by Impey et al. (1998). Their dark mass dominated model and constant mass-to-light ratio model give similar quality fits ($\chi^2_{\min} \approx 3$ to 4 with $N_{\text{dof}} = 1$), but imply $h = 0.44 \pm 0.04$ and $h = 0.65 \pm 0.05$ (for $\Omega_0 = 1$), respectively. Here we focus on the degeneracies in the models of Q0957+561. Since the FGSE model requires a point mass of $\sim 10^{11} M_\odot$ at the center of the galaxy, which appears to be rather unnatural (even if we interpret it as an effective mass rather than a physical BH mass), we would favor the PEM+PS model over the FGSE model unless the FGSE model was found to give a much better fit than the PEM+PS model. At the same time, the large range of h in the PEM+PS model can be significantly reduced if the cluster's mass distribution is more accurately determined from observations in the future (e.g. using AXAF observations, or improved data on weak lensing effects), and/or the galaxy's mass is securely inferred from the measured velocity dispersions of the galaxy using, e.g., realistic stellar dynamics models for the PEM galaxy model. Observational studies of the two optical blobs and two knots (e.g. measurements of their redshifts

and better astrometric and photometric data) will also be useful.

In conclusion, the PEM+PS model of Q0957+561 shows appreciable ($\approx 2 - 3\sigma$) discrepancies with some of the present observational constraints (in particular, the radio jet positions and the optical blob magnification ratio) while it is consistent with many others. For this reason, the determined value of H_0 should be taken with some caution until the discrepancies are resolved. Nevertheless, the modeled mass distributions of the galaxy and the cluster are consistent with the observations of the galaxy and the cluster (in fact, the PEM+PS model was motivated by recent observations of the galaxy and the cluster). This increases the likelihood that this lens can be used to determine H_0 accurately in the future with the aid of better data and more realistic lens models. It is worth mentioning that our present determined value of H_0 is consistent with the independent determination by Impey et al. (1998) using the lens PG 1115+080 and recent determinations from Type Ia supernovae observations, providing the cluster's convergence in the region of the galaxy of Q0957+561 is $\kappa \sim 0.1 - 0.2$ as estimated from recent observations (Chartas et al. 1998; Fischer et al. 1997). For example, if we adopt $\kappa \approx 0.26 \pm 0.08$ (1σ) derived by Bernstein & Fischer (1999) from the Fischer et al. (1997) observation, we find

$$H_0 = 51_{-10}^{+14} \text{ and } 55_{-14}^{+15} \text{ km s}^{-1} \text{ Mpc}^{-1},$$

with and without a constraint on the cluster's mass, respectively. These values of H_0 are in agreement with the values derived from Type Ia Supernovae observations [Branch 1998 ($H_0 = 60 \pm 10$ km s $^{-1}$ Mpc $^{-1}$); Schaefer 1998 ($H_0 = 55 \pm 8$ km s $^{-1}$ Mpc $^{-1}$)] as well as the values obtained by Impey et al. (1998). This could be an indication that both the results from Q0957+561 and PG 1115+080 are on the right track. The coming years will be an exciting period of time for our observational and theoretical efforts to determine more accurately the Hubble constant directly from the time delays of gravitationally lensed systems.

I would like to thank Dr. Bernstein for comments on the HST blobs and providing the revised blob magnification ratio prior to publication and Dr. Barkana for sending a revised version of the article cited in this paper. My special thanks are due to Dr. Turnshek for helpful discussions, careful reading of the manuscript and numerous comments, and his encouragement and support. Financial support from the Andrew Mellon Fellowship is gratefully acknowledged. The anonymous referee provided a very useful review of the paper, which was helpful in clarifying/improving the analysis and presentation.

REFERENCES

Angonin-Willaime, M.-C., Soucail, G., & Vanderriest, C. 1994, *A&A*, 291, 411

Barkana, R., Lehar, J., Falco, E.E., Grogin, N.A., Keeton, C.R., & Shapiro, I.I. 1999, *ApJ*, in press, preprint (astro-ph/9808096) (Ba99)

Bernstein, G., & Fischer, P. 1999, *AJ*, in press, preprint (astro-ph/9903274)

Bernstein, G., Fischer, P., Tyson, J.A., & Rhee, G. 1997, *ApJ*, 483, L79 (Be97)

Branch, D. 1998, *ARA&A*, 36, 17

Chae, K.-H., Khersonsky, V.K., & Turnshek, D.A. 1998, *ApJ*, 506, 80

Chartas, G., Chuss, D., Forman, W., Jones, C., & Shapiro, I. 1998, *ApJ*, 504, 661

Chartas, G., Falco, E.E., Forman, W.R., Jones, C., Schild, R., & Shapiro, I.I. 1995, *ApJ*, 445, 140

Conner, S.R., Lehár, J., & Burke, B.F. 1992, *ApJ*, 387, L61

Dahle, H., Maddox, S.J., & Lilje, P.B. 1994, *ApJ*, 435, L79

Falco, E.E., Gorenstein, M.V., & Shapiro, I.I. 1985, *ApJ*, 289, L1

Falco, E.E., Gorenstein, M.V., & Shapiro, I.I. 1991, *ApJ*, 372, 364

Falco, E.E., Shapiro, I.I., Moustakas, L.A., & Davis, M. 1997, *ApJ*, 484, 70

Fischer, P., Bernstein, G., Rhee, G., & Tyson, J.A. 1997, *AJ*, 113, 521

Garrett, M.A., Calder, R.J., Porcas, R.W., King, L.J., Walsh, D., & Wilkinson, P.N. 1994, *MNRAS*, 270, 457

Garrett, M.A., Walsh, D., & Carswell, R.F. 1992, *MNRAS*, 254, 27

Gorenstein, M.V., Cohen, N.L., Shapiro, I.I., Rogers, A.E.E., Bonometti, R.J., Falco, E.E., Bartel, N., & Marcaide, J.M. 1988, *ApJ*, 334, 42

Gorenstein, M.V., Shapiro, I.I., Corey, B.E., Falco, E.E., Marcaide, J.M., Cohen, N.L., Rogers, A.E.E., Whitney, A.R., Porcas, R.W., & Preston, R.A. 1983, *Science*, 219, 54

Gorenstein, M.V., Shapiro, I.I., Rogers, A.E.E., Cohen, N.L., Corey, B.E., Porcas, R.W., Falco, E.E., Bonometti, R.J., Preston, R.A., Rius, A., & Whitney, A.R. 1984, *ApJ*, 287, 538

Grogin, N.A., & Narayan, R. 1996, *ApJ*, 464, 92; erratum 1996, *ApJ*, 473, 570

Haarsma, D.B., Hewitt, J.N., Lehár, J., & Burke, B.F. 1999, *ApJ*, 510, 64

Impey, C.D., Falco, E.E., Kochanek, C.S., Lehár, J., McLeod, B.A., Rix, H.-W., & Peng, C.Y., & Keeton, C.R. 1998, *ApJ*, 509, 551

Keeton, C.R., Kochanek, C.S., & Falco, E.E. 1998, *ApJ*, 509, 561

Kormann, R., Schneider, P., & Bartelmann, M. 1994, *A&A*, 284, 285

Kundić, T., Turner, E.L., Colley, W.N., Gott III, J.R., Rhoads, J.E., Wang, Y., Bergeron, L.E., Gloria, K.A., Long, D.C., Malhotra, S., & Wambsganss, J. 1997, *ApJ*, 482, 75

Mao, S., & Schneider, P. 1998, MNRAS, 295, 587

Oscoz, A., Mediavilla, E., Goicoechea, L.J., Serra-Ricart, M., & Buitrago, J. 1997, ApJ, 479, L89

Pelt, J., Schild, R., Refsdal, S., & Stabell, R. 1998, A&A, 336, 829

Pijpers, F.P. 1997, MNRAS, 289, 933

Refsdal, S. 1964, MNRAS, 128, 307

Refsdal, S. 1966, MNRAS, 132, 101

Rhee, G. 1991, Nature, 350, 211

Roberts, D.H., Greenfield, P.E., Hewitt, J.N., Burke, B.F., & Dupree, A.K. 1985, ApJ, 293, 356

Romanowsky, A.J., & Kochanek, C.S. 1999, ApJ, in press, preprint (astro-ph/9805080)

Schaefer, B.E. 1998, ApJ, 509, 80

Schild, R., & Smith, R.C. 1991, AJ, 101, 813

Schild, R., & Thomson, D.J. 1997, AJ, 113, 130

Schneider, P., Ehlers, J., & Falco, E.E. 1992, Gravitational Lenses (New York: Springer-Verlag)

Stockton, A. 1980, ApJ, L141

Tonry, J.L., & Franx, M. 1999, ApJ, submitted, preprint (astro-ph/9809064)

Table 1
“Primary” Lensing Constraints¹

Obs. Constraint	value (uncertainty)	reference(s)
$\Delta\alpha(A_5 - A_1)$ (mas) ²	16.6 (0.1)	1
$\Delta\delta(A_5 - A_1)$ (mas) ²	45.6 (0.1)	1
$\Delta\alpha(B_5 - B_1)$ (mas) ²	18.32 (0.07)	1
$\Delta\delta(B_5 - B_1)$ (mas) ²	55.8 (0.2)	1
M_1 at A_5 ³	1.15 (0.03)	1
M_2 at A_5 ³	-0.56 (0.03)	1
$\phi_1(^{\circ})$ at A_5 ³	18.76 (0.04)	1
$\phi_2(^{\circ})$ at A_5 ³	107 (7)	1
M_1 at A_1 ³	1.27 (0.03)	1
M_2 at A_1 ³	-0.58 (0.04)	1
$\Delta\alpha(A_1 - B_1)$ (")	-1.25254 (0.00004)	1, 2
$\Delta\delta(A_1 - B_1)$ (")	6.04662 (0.00004)	1, 2
Rel. Mag. (B_1/A_1)	0.747 (0.015)	3
$\Delta\alpha(G' - B_1)$ ⁴	0.181 (0.001)	4
$\Delta\delta(G' - B_1)$ ⁴	1.029 (0.001)	4

NOTE—(1) All of the positions are for J1950.0. (2) See Table 2 for the correlation coefficients. (3) See Table 3 for the correlation coefficients. (4) Since the VLBI position of G' is consistent with the HST position by Bernstein et al. (1997) at a 10 mas level, we have chosen to use this position. However, the model fit is unaffected if the HST position is used.

REFERENCES—(1) Barkana et al. (1998); (2) Falco, Gorenstein, & Shapiro 1991; (3) Conner, Lehár, & Burke 1992; (4) Gorenstein et al. 1983

Table 2
Correlation Coefficients for Radio Jet Positions¹

	$\Delta\alpha(A_5 - A_1)$	$\Delta\delta(A_5 - A_1)$	$\Delta\alpha(B_5 - B_1)$	$\Delta\delta(B_5 - B_1)$
$\Delta\alpha(A_5 - A_1)$	1.00			
$\Delta\delta(A_5 - A_1)$	0.26	1.00		
$\Delta\alpha(B_5 - B_1)$	-0.40	0.27	1.00	
$\Delta\delta(B_5 - B_1)$	-0.12	0.19	0.36	1.00

NOTE—(1) Adapted from Barkana et al. (1998)

Table 3
Correlation Coefficients for Magnification Constraints¹

	M_1 at A_5	M_2 at A_5	ϕ_1 at A_5	ϕ_2 at A_5	M_1 at A_1	M_2 at A_1
M_1 at A_5	1.00					
M_2 at A_5	0.05	1.00				
ϕ_1 at A_5	-0.27	0.25	1.00			
ϕ_2 at A_5	-0.34	-0.74	-0.16	1.00		
M_1 at A_1	-0.95	-0.02	0.20	0.16	1.00	
M_2 at A_1	-0.06	0.985	0.31	-0.70	0.09	1.00

NOTE–(1) Adapted from Barkana et al. (1998)

Table 4
“Secondary” Lensing Constraints^{1,2}

Obs. Constraint	value (uncertainty)	reference
$\Delta\alpha$ (Blob 2) (")	1.72 (0.05)	1
$\Delta\delta$ (Blob 2) (")	0.98 (0.05)	1
$\Delta\alpha$ (Blob 3) (")	-2.70 (0.05)	1
$\Delta\delta$ (Blob 3) (")	4.48 (0.05)	1
Rel. Mag. (Blob 2/Blob 3)	0.41 (^{+0.14} _{-0.11})	2
$\Delta\alpha$ (Knot 1) (")	0.13 (0.05)	1
$\Delta\delta$ (Knot 1) (")	-1.53 (0.05)	1
$\Delta\alpha$ (Knot 2) (")	-0.29 (0.05)	1
$\Delta\delta$ (Knot 2) (")	-1.41 (0.05)	1
Rel. Mag. (Knot 1/Knot 2)	0.76 (^{+0.68} _{-0.36})	1

NOTE–(1) The redshifts of the objects are unknown at present. (2) All of the positions are relative to the core of the quasar B (e.g. component B_1) and for J1950.0.

REFERENCE–(1) Bernstein et al. (1997); (2) Bernstein (1998, private communication)

Table 5
Fitted Values of the Model Parameters¹

Parameter	Best-fit value	$\Delta\chi^2 = \bar{\chi}_{\min}^2$ range
ν_1	1.72	$1.62 \lesssim \nu_1 \lesssim 1.80$
$r_1 (h^{-1} \text{ kpc})$	10^{-4} (fixed)	—
$\Sigma_1 (10^{10} \text{ M}_\odot \text{ kpc}^{-2})$	723.4	$284.5 \lesssim \Sigma_1 \lesssim 1754.$
ϵ_1	0.184	$0.007 \lesssim \epsilon_1 \lesssim 0.377$
$\theta_1 (\text{°})$	64.0	$5.7 \lesssim \theta_1 \lesssim 166.0$
ν_2	2 (fixed)	—
$r_2 (h^{-1} \text{ kpc})$	15 (fixed)	—
$\Sigma_2 (10^{10} \text{ M}_\odot \text{ kpc}^{-2})$	0.246	$0.164 \lesssim \Sigma_2 \lesssim 0.389$
$d_{12} (\text{''})$	9.	$5. \lesssim d_{12} \lesssim 13.$
PA ₁₂ (°)	51.8	$38.0 \lesssim \text{PA}_{12} \lesssim 60.0$
z_{blob}	1.43	$1.41 \lesssim z_{\text{blob}} \lesssim 1.47$
z_{knot}	1.34	$1.22 \lesssim z_{\text{knot}} \lesssim 1.54$

NOTE—(1) The source positions of the core, the jet, the blob, and the knot are not included here. The total number of *free* parameters including the eight source positions is 17.

Table 6
Individual χ^2 Contributions from the Observational Constraints

Constraints	N _{constraint}	χ^2	(χ^2 /N _{constraint})
Jet positions	4	19.00	(4.75)
Core positions	2	0.00	(0.00)
G1 positions	2	0.05	(0.03)
Magnification constraints	6	18.65	(3.11)
Core magnification ratio	1	0.08	(0.08)
“Blob 2” positions	2	3.24	(1.62)
“Blob 3” positions	2	0.18	(0.09)
Blob magnification ratio	1	8.26	(8.26)
“Knot 1” positions	2	0.00	(0.00)
“Knot 2” positions	2	0.00	(0.00)
Knot magnification ratio	1	0.19	(0.19)
Total	25	49.6	

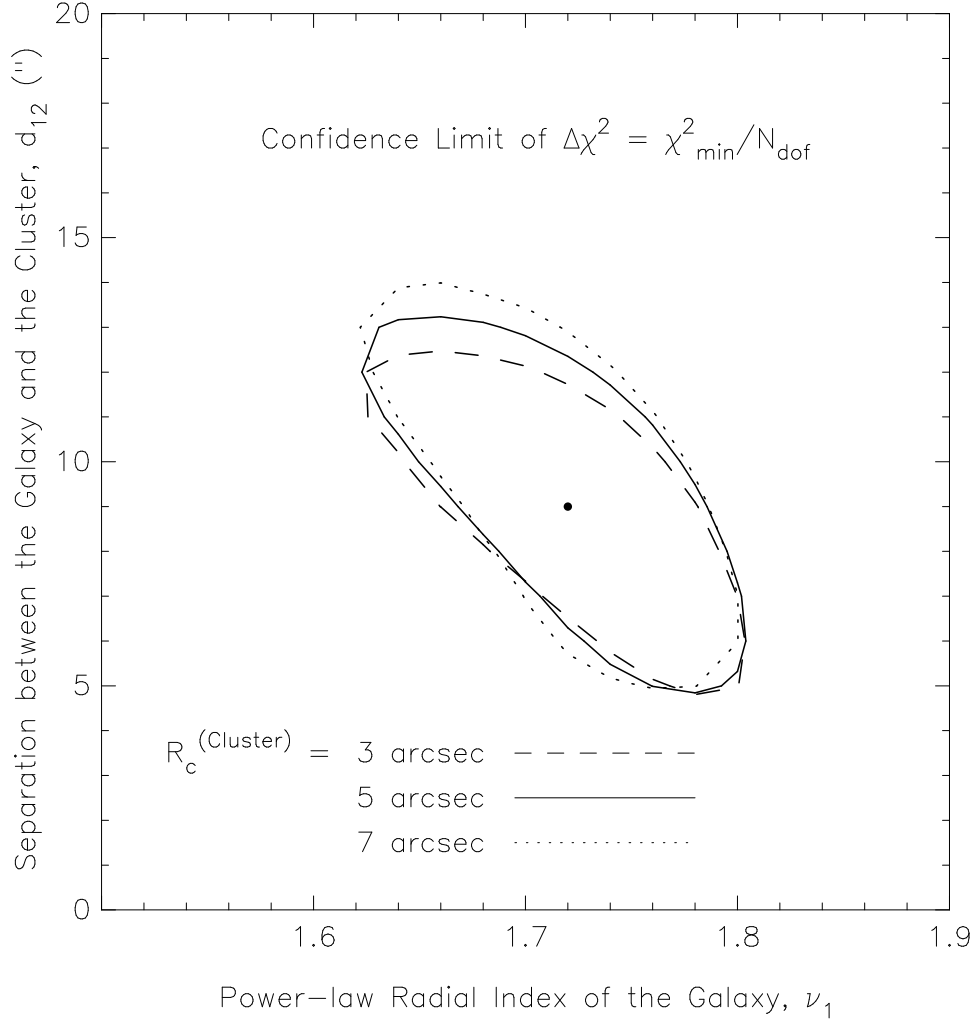
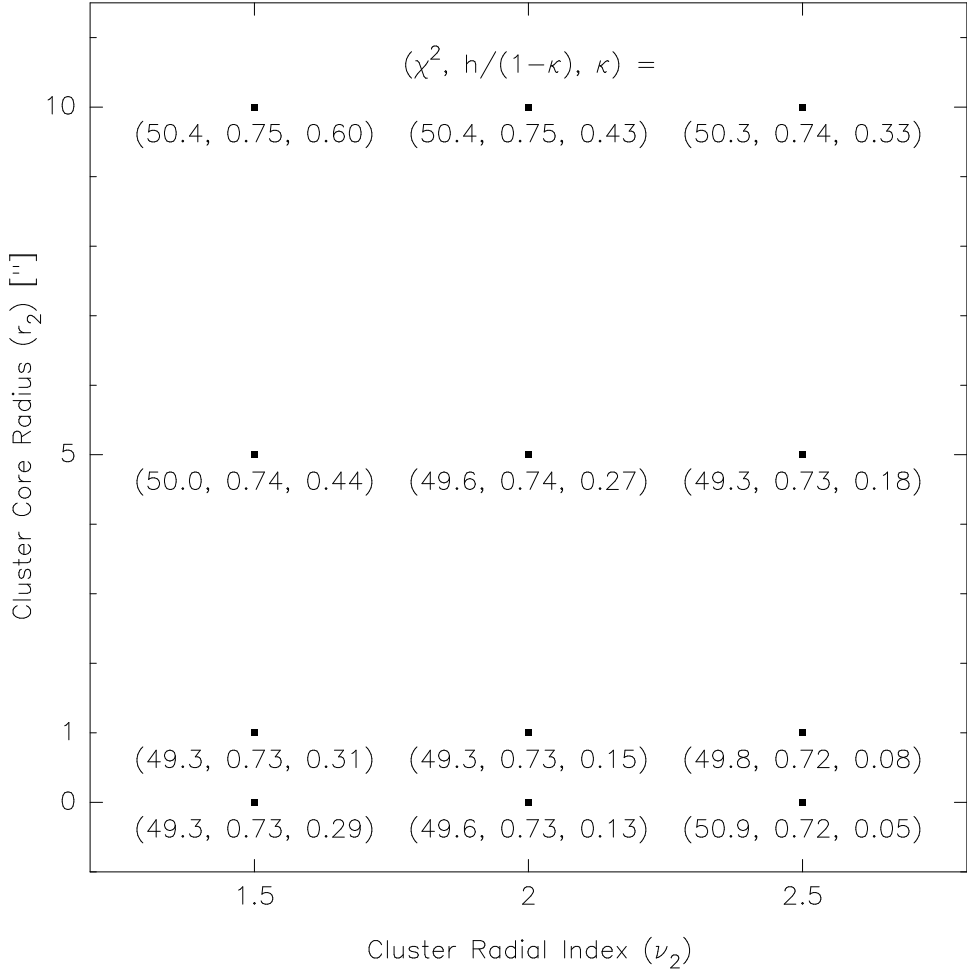


Fig. 1.— A confidence region of parameter space defined by $\Delta\chi^2 = \bar{\chi}^2_{\min}$ (see §4) around the best-fit model ($\nu_1 = 1.72$ and $d_{12} = 9''$). The two-dimensional parameter space is spanned by the radial index of the lensing galaxy (ν_1) and the (projected) separation between the galaxy and the cluster (d_{12}). The cluster is represented by a power-law mass sphere with a non-singular core in the basic model (eq. [2]), and here a fixed value of $\nu_2 = 2$ (“isothermal” distribution) is used. To illustrate how the confidence region is affected when the value of the cluster’s core radius is varied from the best-estimated value of 5'' (Fischer et al. 1997), core radii of 3'' and 7'' are considered as well as the best-estimated value. We find that the confidence region is altered only slightly as the core radius is varied.



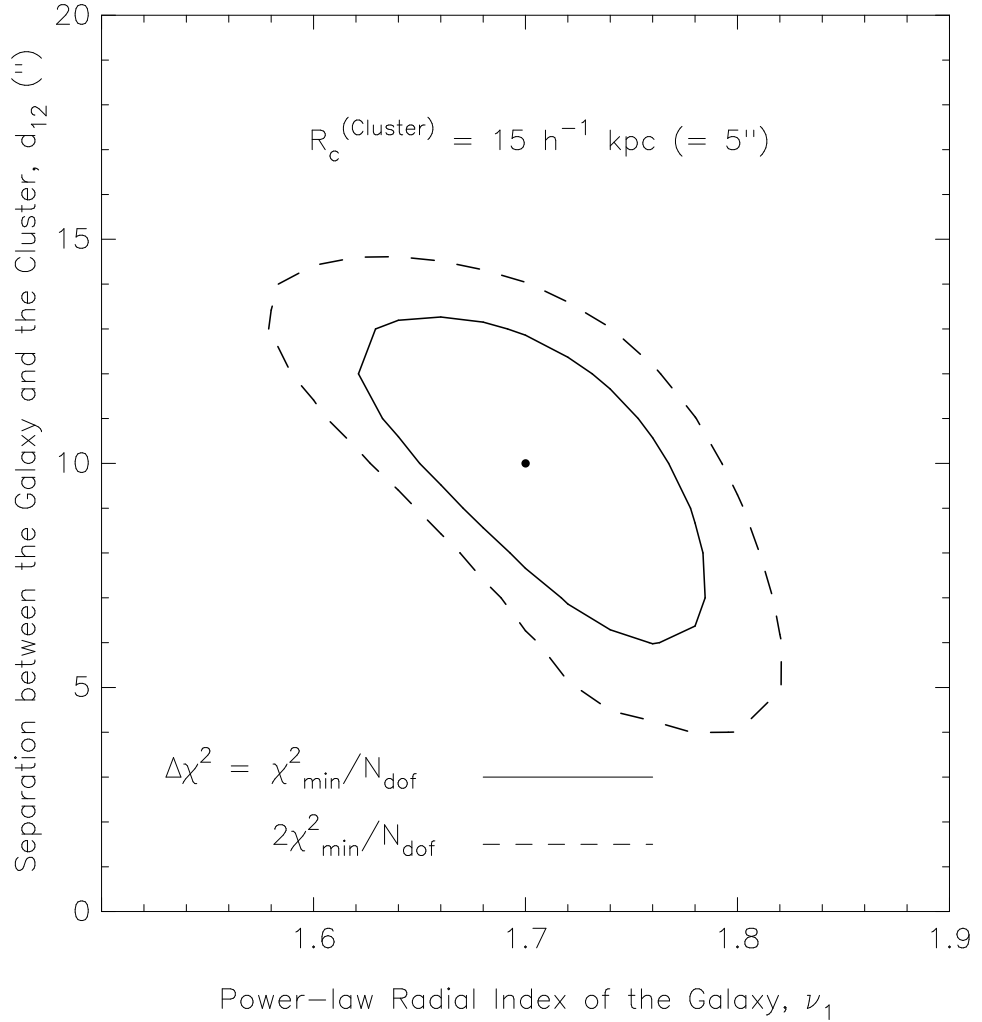


Fig. 3.— Confidence regions, in the same parameter space as in Figure 1, of the model with the cluster core radius of 5''. Here the cluster's mass is constrained using the observationally derived value by Fischer et al. 1997. The parameter space is slightly better constrained compared with the case (Fig. 1) when the cluster's mass is not used as an observational constraint. In fact, if the cluster's mass were determined more accurately by observations, the confidence region of parameter space could be reduced significantly, thereby reducing the allowed range of H_0 .

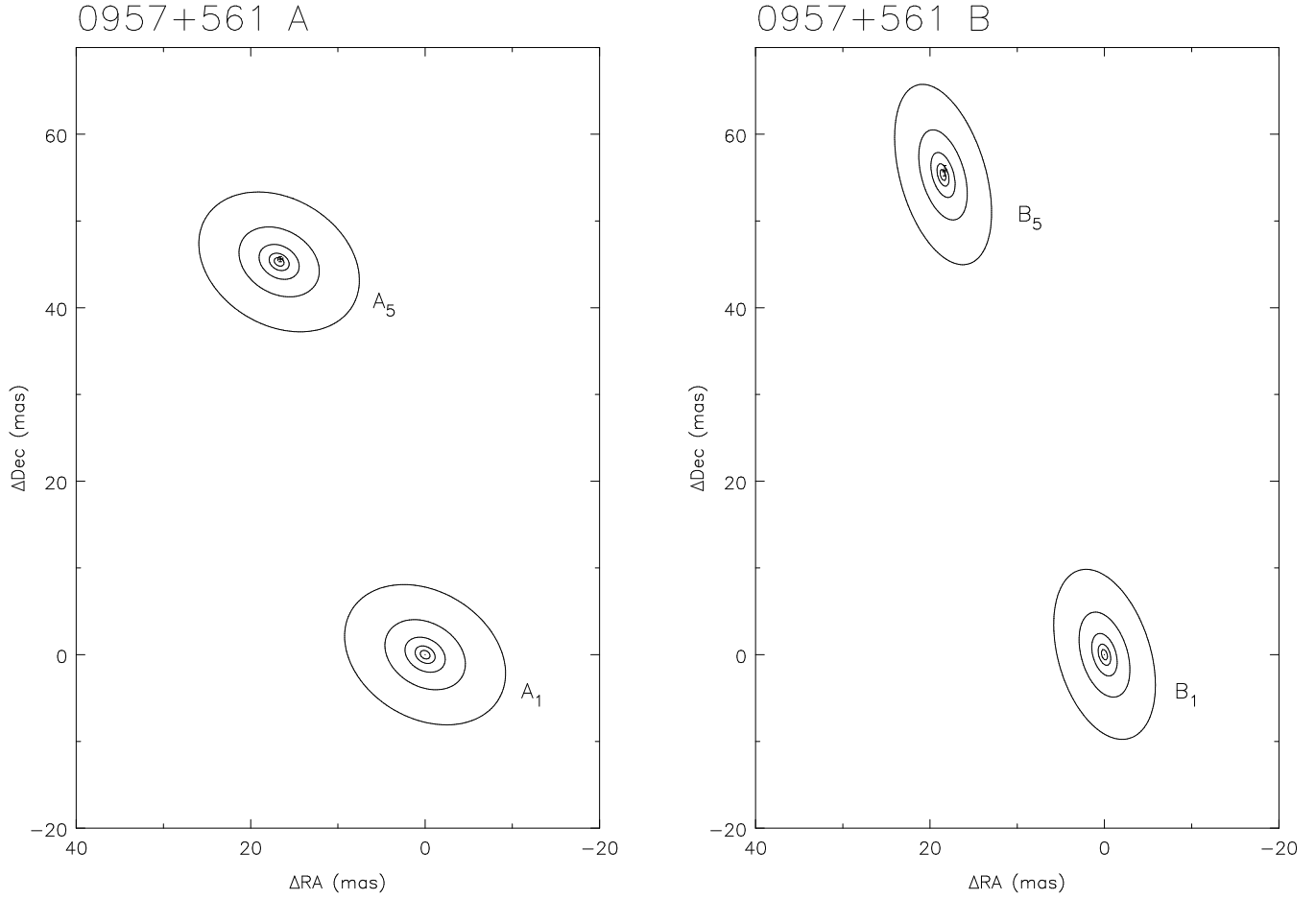


Fig. 4.— Theoretical images of the radio core and the brightest radio jet of Q0957+561 for the best-fit model (see Table 5). The five contour levels for the core and the jet correspond to 1, 2, 4, 8, and 16 pc from their respective centers on the source plane. The observed jet positions relative to their respective cores are also shown. The error bars represent 3σ uncertainties. North is on the top and east is to the left.

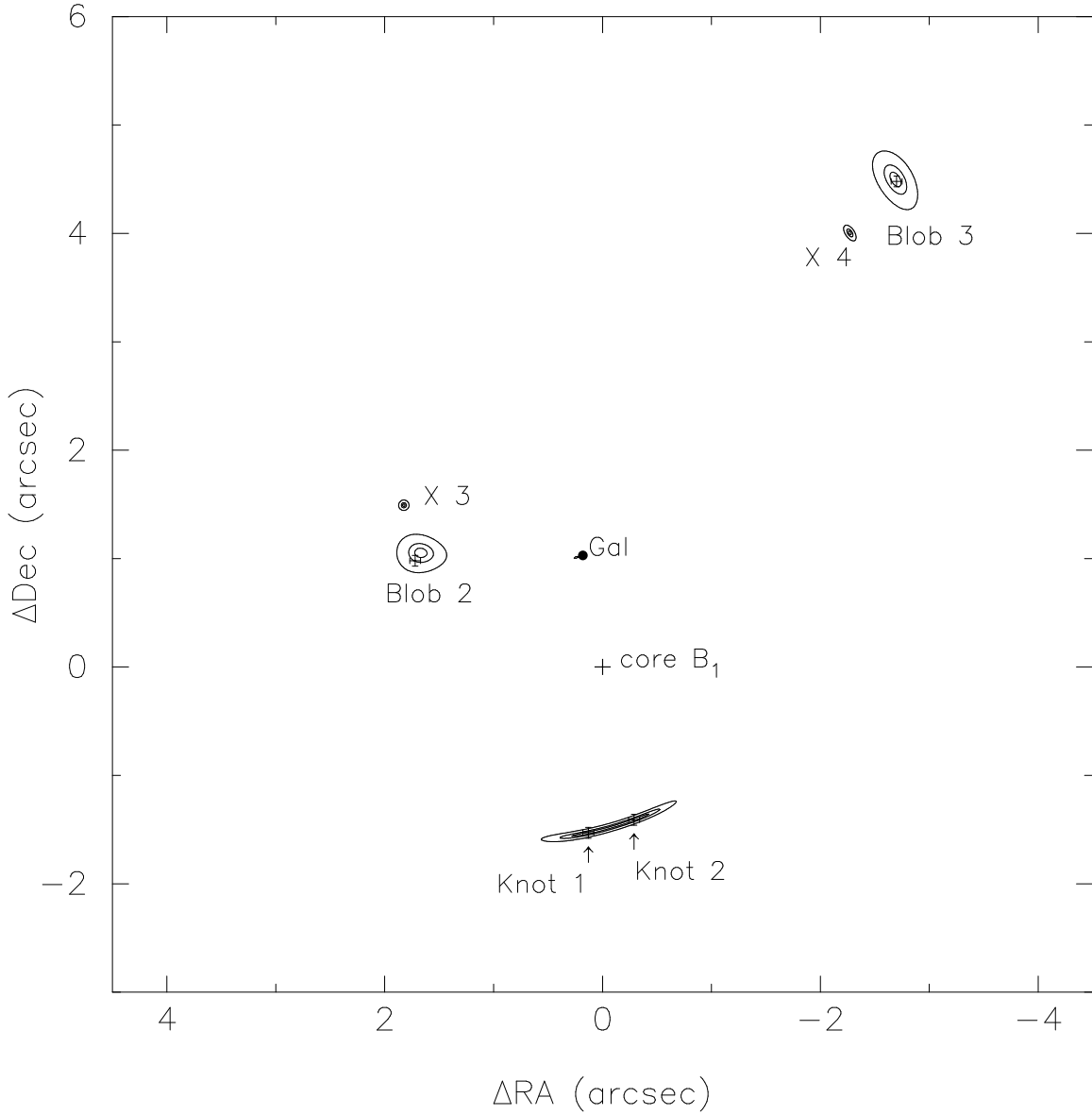


Fig. 5.— Theoretical images of the optical blob and knot of Q0957+561 for the best-fit model (see Table 5). The three contour levels for the blob correspond to 100, 200, and 400 pc at its estimated redshift of $z = 1.43$. The three contour levels for the knot correspond to 25, 50, and 100 pc at its estimated redshift of $z = 1.34$. The observed positions of the blobs and knots (Table 4) are also shown with 1σ error bars. The objects marked “X 3” and “X 4” are two weak additional images of the knot predicted by the lens model. North is on the top and east is to the left.